Progress In Electromagnetics Research, PIER 82, 95–107, 2008

COMPUTATION OF ELECTROMAGNETIC DOSIMETRY FOR HUMAN BODY USING PARALLEL FDTD ALGORITHM COMBINED WITH INTERPOLATION TECHNIQUE

Y. Liu, Z. Liang, and Z.-Q. Yang

College of Physical Electronics
University of Electronic Science and Technology of China
Chengdu 610054, China

Abstract—To enhance the flexibility of the parallel FDTD for the analysis of the bio-electromagnetic problems, a universal and efficient interpolation technique based on the super-absorbing boundary principle is presented, which can improve the interpolation accuracy and ensure the stability of the parallel FDTD iterative procedure. Using this technique, we calculate the SAR (Specific Absorption Rate) values in the head for two different human-body postures. In the iteration procedure of parallel FDTD, the data are exchanged between adjacent subdomains with the interpolation technique. Thus, the meshes can be created in local coordinates, which makes it convenient to build the human model in the different posture and use position for FDTD computing. The results show that the change of human-body posture only brings about a slight decrease (within 6.8%) in the peak SAR values, whereas the SAR values in the brain, as a critical organ, are sensitive to the change of the body posture, and it increases by 28% at maximum for the 1-g averaged peak SAR.

1. INTRODUCTION

With the rapid development of the wireless communication technology and the widespread use of mobile phone [1–6], there has been increasing public concern about the influence of the electromagnetic (EM) radiation on the human body, and SAR has been recognized as one of the most significant parameters describing the electromagnetic field interaction with the human body [7]. Since it is very difficult to quantify the SAR directly in a living human, dosimetry is compelled to rely mainly on computer simulation with high-resolution numerical

human models derived from magnetic-resonance imaging (MRI) data. The finite difference time domain (FDTD) algorithm is currently the most widely accepted means for numerical dosimetry [8, 9]. By discretizing space into a number of cells, and by assigning each cell a corresponding permittivity and conductivity, this algorithm offers great flexibility in modeling the heterogeneous structures of anatomical tissues and organs [10–14]. As the use of MRI-based millimeter high-resolution human models requires huge amount of memory and long simulation time, it could place the solution of the problems beyond the capabilities of any single computer. To overcome the bottlenecks of the computational power and storage requirement, the exploitation of parallel FDTD has been presented for whole-body numerical dosimetry in the last fewer years [15, 16].

In the traditional parallel FDTD algorithm, the whole computational space is decomposed into several subdomains in uniform Cartesian coordinates, and the tangential field components are exchanged at the subdomain boundaries [17, 18]. However, unlike the regular electromagnetic structures, the human body has various changes in the posture, such as the standard standing, the head rotating forward or arms stretching vertically up. Besides, the mobile phone in use can have inconsistent position, e.g., tilted by 30°, 45° or 60°. Thus, some of the subdomains are not parallel with the Cartesian coordinate plane. As the discretization grids of the traditional FDTD are usually rectangular in shape, it does not produce accurate results for whole-body numerical dosimetry owing to the staircasing approximation. In view of the factor that the mobile phone is the chief radiation source, the staircasing introduces significant errors. To avoid compromising accuracy, a scheme by which the human model is rotated via coordinate conversion is adopted to fit the handset antenna to FDTD lattices in literature [19]; nevertheless, this scheme increases, to a great extent, the complexity of the FDTD algorithm, and moreover, when the posture of human body further changes, it is very difficult to build the human model via coordinate conversion.

In this paper, to enhance the flexibility of the parallel FDTD for the analysis of the bio-electromagnetic problems, a universal and efficient interpolation technique based on the domain decomposition parallel FDTD (DD-PFDTD) is presented, which can improve the interpolation accuracy between subdomains. Thus, the computational space is divided largely according to the features of the original problem, which makes it convenient to build the human model. Using this approach, we calculate the SAR values in the head for two different postures: the standard standing and arms stretching up, when the human body is exposed to the electromagnetic radiation from a mobile

phone. Moreover, we also analyze the effect of human-body posture on the SAR in the user head in detail.

2. INTERPOLATION TECHNIQUE FOR PARALLEL FDTD

In certain circumstances, it is difficult to find a uniform mesh scheme, which can exactly describe all the subdomains of parallel FDTD, such as the bio-electromagnetic modeling mentioned above. To break through the drawback, the DD-PFDTD combined with interpolation technique is proposed. Thus, the computational space can be divided into several subdomains corresponding to the posture of human body and the use position of mobile phone. The meshes are created in local coordinates. In each subdomain, the FDTD computation is carried out independently in local meshes and local time step [20]. During the iteration process of FDTD, the adjacent subdomains in uniform system of coordinates exchange directly the tangential field data at the boundaries, and those in different system of coordinates have an overlapping boundary region, and the interpolation technique with overlapped meshes is applied. It is obvious that the key step of this approach is the data interpolating process between subdomains, which must ensure the stability and accuracy of the FDTD iterative procedure.

On account of the simplicity and usefulness, the linear interpolation is widely employed for the DD-PFDTD [21]. To reduce the interpolating errors, one technique is to shorten the grid increment of the overlapping domain, yet will bring about the rapid increase of computation and storage. Therefore, it is necessary to find an effective means, which can reduce the linear interpolation errors on condition that the grid increment retains invariable.

Based on the principle proposed in literatures [22, 23], if the boundaries of subdomains are regarded as generalized absorbing boundaries, we can correct the interpolation errors on the second layer of meshes. In the three-dimensional case, as shown in Figure 1, the magnetic fields on the outermost layer of the subdomain, $H_y(i,\ j,\ k+1/2)$ and $H_z(i,\ j+1/2,\ k)$ are obtained by the linear interpolation from the adjacent subdomain. The corresponding interpolation errors are

$$e_1^y = \tilde{H}_y^{n+\frac{1}{2}}(i,j,k+1/2) - H_y^{n+\frac{1}{2}}(i,j,k+1/2) \tag{1}$$

$$e_1^z = \tilde{H}_z^{n+\frac{1}{2}}(i,j+1/2,k) - H_z^{n+\frac{1}{2}}(i,j+1/2,k) \tag{2}$$

where $H_y^{n+1/2}$ and $H_z^{n+1/2}$ stand for the exact magnetic fields, $\tilde{H}_y^{n+1/2}$ and $\tilde{H}_z^{n+1/2}$ stand for the interpolated magnetic fields.

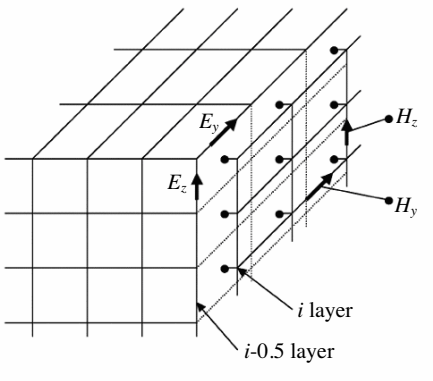

Figure 1. The three-dimensional FDTD lattices.

At the mesh nodes of layer $(i-1/2)$, the electric fields can be obtained from the FDTD iterative computation.

$$\begin{aligned}\hat{E}_y^{n+1}(i-1/2,j+1/2,k) &= E_y^n(i-1/2,j+1/2,k)\\ &-\frac{\Delta t}{\varepsilon\Delta x}\left[\tilde{H}_z^{n+1/2}(i,j+1/2,k)-H_z^{n+1/2}(i-1,j+1/2,k)\right]\\ &+\frac{\Delta t}{\varepsilon\Delta z}\left[H_x^{n+1/2}(i-1/2,j+1/2,k+1/2)\right.\\ &\left.-H_x^{n+1/2}(i-1/2,j+1/2,k-1/2)\right] \qquad (3)\end{aligned}$$

Considering (2), then (3) can be rewritten as

$$\hat{E}_y^{n+1}(i-1/2,j+1/2,k) = E_y^{n+1}(i-1/2,j+1/2,k) - \frac{\Delta t}{\varepsilon\Delta x}e_1^z \qquad (4)$$

By the same means, we have

$$\hat{E}_z^{n+1}(i-1/2,j,k+1/2) = E_z^{n+1}(i-1/2,j,k+1/2) + \frac{\Delta t}{\varepsilon\Delta x}e_1^y \qquad (5)$$

where E_y^{n+1} and E_z^{n+1} stand for the exact value, $\hat{E}_y^{n+1}$ and $\hat{E}_z^{n+1}$ stands for the calculated value including the interpolation errors e_1^y and e_1^z.

The electric fields on the $(i-1/2)$ layer of meshes can also be obtained by interpolation.

$$\tilde{E}_y^{n+1}(i-1/2,j+1/2,k) = E_y^{n+1}(i-1/2,j+1/2,k) + e_2^y \qquad (6)$$

$$\tilde{E}_z^{n+1}(i-1/2,j,k+1/2) = E_z^{n+1}(i-1/2,j,k+1/2) + e_2^z \qquad (7)$$

where $\tilde{E}_y^{n+1}$ and $\tilde{E}_z^{n+1}$ express the electric field values obtained by interpolation, e_2^y and e_2^z are the interpolation errors. Because the same interpolation process is applied to magnetic fields as well as electric fields, e_1 and e_2 should satisfy a certain relationship. According to the super-absorbing boundary principle in literature [11], we can get

$$e_2^y \sin\left(\frac{\omega\Delta t}{2}\right) = \frac{\Delta t}{\varepsilon\Delta x}\exp\left[J\left(\frac{\omega\Delta t}{2}+\frac{k_x\Delta x}{2}\right)\right]\times e_1^z \sin\left(\frac{k_x\Delta x}{2}\right) \quad (8)$$

$$e_2^z \sin\left(\frac{\omega\Delta t}{2}\right) = -\frac{\Delta t}{\varepsilon\Delta x}\exp\left[J\left(\frac{\omega\Delta t}{2}+\frac{k_x\Delta x}{2}\right)\right]\times e_1^y \sin\left(\frac{k_x\Delta x}{2}\right) \quad (9)$$

where J is the unit imaginary number, ω is the angle frequency, k_x is the wave number along the x axis. In FDTD algorithm, Δx should satisfy $\Delta x \le \lambda/10$, thus we have

$$k_x\Delta x \ll 1, \quad \omega\Delta t \ll 1 \quad (10)$$

Combining (4)–(9), and make some approximation by (10), we can get the modified interpolation formulae as follows:

$$E_y^{n+1}(i-1/2, j+1/2, k) = \frac{\hat{E}_y^{n+1}(i-1/2, j+1/2, k)+\rho\tilde{E}_y^{n+1}(i-1/2, j+1/2, k)}{1+\rho} \quad (11)$$

$$E_z^{n+1}(i-1/2, j, k+1/2) = \frac{\hat{E}_z^{n+1}(i-1/2, j, k+1/2)+\rho\tilde{E}_z^{n+1}(i-1/2, j, k+1/2)}{1+\rho} \quad (12)$$

where $\rho = \upsilon\Delta t/\Delta x$, υ is phase velocity and $\upsilon = 1/\sqrt{\varepsilon\mu}$.

Utilizing (11)–(12), the interpolation errors can be considerably reduced. Therefore, for the DD-PFDTD, the primary steps of interpolation are as follows:

1) the magnetic fields or electric fields on the first layer of meshes are obtained from the adjacent subdomain by using the linear interpolation.

2) The electric fields or magnetic fields on the second layer of meshes are obtained by the same interpolation method and FDTD iterative calculation simultaneity, and then (11)–(12) are used to correct the interpolation errors.

After finishing these steps, the accuracy of the exchanged data between subdomains can be ensured. However, the interpolation is an indirect method for data exchange, which will bring on the lower parallel efficiency as compared with the traditional method in which data are directly transferred. In order to improve the parallel efficiency,

we adopt a novel MPI-OpenMP hybrid FDTD approach, which introduces task parallelization at the basis of the data parallelization of the traditional DD-PFDTD. The Message Passing Interface (MPI) library is used in conjunction with OpenMP multithreading to achieve two-level parallelization of the data and tasks. By using OpenMP compiler directives (**#pragma omp parallel sections**), the interpolation between subdomains and the iteration within subdomains are divided into two relatively independent subtasks, which can be parallelized by going multithreaded. In literature [21], we analyzed the parallel performance of this approach in detail. In fact, considering that modern CPUs give directly support to multithreading or multiple tasks from the hardware, the overlapping operation of the interpolation and iteration can availably be achieved with the use of OpenMP multithreading as the second level parallelization, which will ensure the parallel performance of the DD-PFDTD with interpolation technique.

3. NUMERICAL MODELS

In order to discuss the effect of the human-body posture on the SAR in the head of the handset user, a realistic whole-body human model has been used, which is developed from MRI scans of a male volunteer of height 176 cm and weight 73 kg. It consists of 30 types of tissue and has a resolution of 2 mm. The tissue classification of the FDTD cell is decided by the major tissue in the cell. The electrical properties and densities of the tissues which are derived from literature [24] are adopted in FDTD computation. Figure 2 shows a visualization of the human model in two postures: one is the standard standing, another is arms stretching vertically up.

The handset model used is the Generic mobile phone [25], which is proposed by Food and Drug Administration for an international comparison study, and is composed of a monopole antenna and a solid plastic body with 102 mm high, 42 mm wide, and 21 mm thick. A perfect electrical conductor (PEC) material with 1 mm thick is embedded in the body of the Generic mobile phone, as shown in Figure 3. The length of the antenna is 71 mm for the operating frequency of 835 MHz. The handset is set to touch the left ear of the human head.

4. RESULTS AND DISCUSS

Considering the posture and position in use, the FDTD simulations are performed in three cases: 1) the standard standing with the head tilted forward by 45° and the mobile phone in the vertical use position;

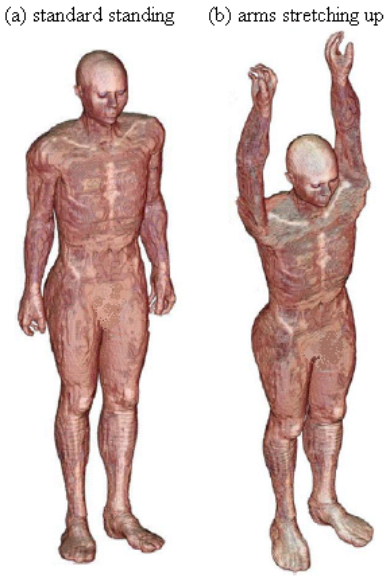

Figure 2. Two different postures of the human model.

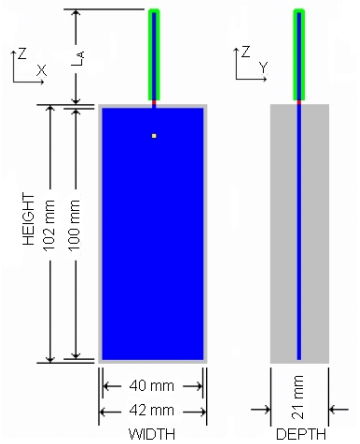

Figure 3. The generic mobile phone model.

2) the same as the case-1 in the posture and the mobile phone tilted backward by 30° relative to vertical; 3) arms stretching vertically up with the head tilted forward by 45° and the same as the case-2 in the use position of the mobile phone.

Due to being tilted, the principal axes of the head and mobile

phone are not parallel with the rest of the human model, which brings on it difficult to discretize accurately the computational domain by using a uniform mesh scheme. According to the principle proposed in Section 2, we regard the head and mobile phone as two independent subdomains. Considering that the thickness of the PEC material is 1 mm, the local meshes with $1 \times 1 \times 1$ mm are created in the mobile phone. Thus, the problem can be solved by the DD-PFDTD with interpolation technique.

Figures 4(a)–(c) shows SAR distributions for three cases in the horizontal section of the human head close to the feeding point of the antenna. We can see that there are relatively obvious variations between adjacent cells of the tissues with different dielectric characteristics, and the maximum SAR values are located in the external ear (pinna) and the skin tissue layers of the head. For the same numerical model, we previously reported the SAR distributions for the case-1 using the traditional DD-PFDTD [26], which agree well (difference within 3.2%) with our present results. This verifies indirectly the validity of the parallel FDTD code with interpolation technique for the SAR calculations.

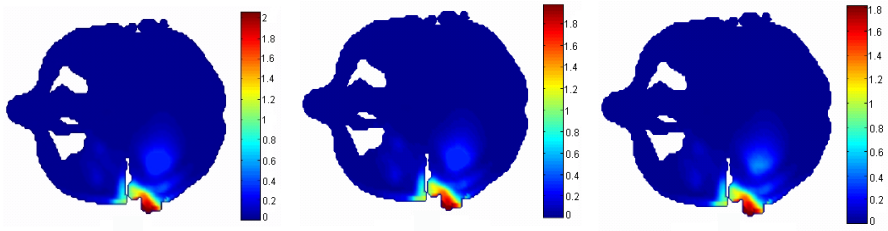

Figure 4. The SAR distributions for three cases in the horizontal section of human head. (a) Standard standing and vertical use position. (b) Standard standing and tilted 30°. (c) Arms stretching up and tilted 30°.

According to the ANSI/IEEE Std C95-1-1999 and the ICNIRP Guidelines, the dosimetric compliance of mobile phones requires the assessment of the maximum SAR (averaged over 1-g of tissue or 10-g of tissue) in the human head. We have made the relevant calculations and give the spatial peak SAR in Table 1. The 1- and 10-g averaged spatial peak SARs were derived by shifting a cube of $1 \times 1 \times 1$cm and a cube of $2.2 \times 2.2 \times 2.2$ cm, respectively, across the head volume and computing SARs averaged over the cubes at every position by using $SAR = \sigma E^2/2\rho$ (ρ: tissue density).

Table 1. Comparison of the 1- and 10-g averaged peak SARs in the head for three cases. Antenna output: 0.27 W.

	Standard standing Vertical	Standard standing Tilted 30°	Arms up Tilted 30°	Posture effect
1 g peak SAR (W/kg)	2.16	1.87	1.82	−2.7%
10 g peak SAR (W/kg)	1.32	1.12	1.06	−5.3%

In the SAR calculations above, the pinna is considered as part of the 1- or 10-g SAR averaging volumes. Because the pinna is usually the tissue closest to the feeding point of the handset antenna, the highest SAR value only for one FDTD cell (1-voxel SAR) is usually found in the pinna, consequently, averaging volumes that include pinna tissue will produce higher SAR. Exclusive of the pinna, we calculate the 1- and 10-g averaged spatial peak SARs in the head, and the results are shown in Table 2.

Table 2. Exclusive of the pinna, comparison of the 1- and 10-g averaged peak SARs in the head for three cases. Antenna output: 0.27 W.

	Standard standing Vertical	Standard standing Tilted 30°	Arms up Tilted 30°	Posture effect
1 g peak SAR (W/kg)	1.27	1.09	1.05	−4.1%
10 g peak SAR (W/kg)	0.76	0.65	0.61	−6.8%

It can be seen from Tables 1 and 2 that the higher peak SAR occurred in the vertical use position, which is similar to the results obtained by using the isolated head model in literature [27]. Moreover, the safety limit (1.6 W/kg for SAR_{1g}) can be exceeded if the pinna is included in the averaging volume. As for the effect of body posture, we find that the peak SAR values decrease slightly (within 6.8%) in arms up posture as compared with those in standard standing posture for the same use position (tilted 30°).

In order to better identify the electromagnetic absorption characteristics in the major organ of the head and elucidate the body posture effect, we compared the SAR values averaged over 1-g, 10-g and the whole organ for the brain in Table 3.

Table 3. Comparison of the 1-, 10-g averaged peak SARs and the whole organ averaged SARs inside the brain for three cases. Antenna output: 0.27 W.

	Standard standing Vertical	Standard standing Tilted 30°	Arms up Tilted 30°	Posture effect
1 g peak SAR (W/kg)	0.252	0.237	0.303	28%
10 g peak SAR (W/kg)	0.137	0.128	0.152	19%
Average SAR (mW/kg)	16.8	19.7	22.3	13.4%

It is worth noting that a trend of increasing for both the 1-, 10-g averaged peak SARs and the whole organ averaged SAR inside the brain in arms up posture, although the different use position (vertical or tilted 30°) is employed. The maximum posture effect reaches 28% for the 1-g averaged peak SAR in the brain, which implies that the posture of arms stretching up plays a significant role in the EM energy absorption, and increases the maximum SAR level in the brain. However, the quantitative SAR values obtained above are apparently lower than the safety limits (1.6 W/kg for SAR_{1g} and 2 W/kg for SAR_{10g}). This also implies an insignificant effect of the posture on the head when considering the spatial peak SAR assessment. Therefore, the SAR values derived from the standard standing posture should be appropriate, to a certain extent, for the evaluation of the SAR occurring in a real-life handset user, as required by the ANSI/IEEE or ICNIRP guidelines.

5. CONCLUSIONS

In this paper, we introduce a universal and efficient interpolation technique based on the super-absorbing boundary principle, which can improve the interpolation accuracy and ensure the stability of the FDTD iterative procedure. Using this technique, we have developed

a novel MPI-OpenMP hybrid DD-PFDTD computation system for investigating the human-body posture effect on the SAR deposition for the mobile phone. Since a complicated problem is divided into several relatively independent sub-problems, it is convenient to build the human model in the different posture and use position for FDTD computing. As a result, we have found that there is no obvious difference for the peak SARs in the head between the standard standing and arms stretching up posture, whereas the SAR values in the brain, as a critical organ, are sensitive to the change of the body posture, and it increases by 28% at maximum for the 1-g averaged peak SAR. These results further confirm the complex interaction of EM energy with human body consisting of multiple tissue types with varying dielectric properties.

ACKNOWLEDGMENT

This work was supported in part by the National Natural Science Fund (60571020) of P. R. China. The authors would like to thank Dr. M. Yang and Dr. Y. K. Sun for their useful discussions and suggestions during the development of the human body model.

REFERENCES

1. Liu, W.-N., J.-K. Xiao, S. Zhang, and Y. Li, "A novel PBG planar inverted-F antenna for wearable system," *Journal of Electromagnetic Waves and Applications*, Vol. 20, No. 5, 615–622, 2006.
2. Chen, Y. B., X. F. Liu, Y. C. Jiao, and F. S. Zhang, "A frequency reconfigurable CPW-fed slot antenna," *Journal of Electromagnetic Waves and Applications*, Vol. 21, No. 12, 1673–1678, 2007.
3. Peng, L. and C. -L. Ruan, "A microstrip fed monopole patch antenna with three stubs for dual-band WLAN applications," *Journal of Electromagnetic Waves and Applications*, Vol. 21, No. 15, 2359–2369, 2007.
4. El-Fishawy, N., M. Shokair, and W. Saad, "Proposed Mac protocol versus IEEE 802.15.3a for multimedia transmission over UWB networks," *Progress In Electromagnetics Research B*, Vol. 2, 189–206, 2008.
5. Min, K.-S., M.-S. Kim, C.-K. Park, and M. D. Vu, "Design for PCS antenna based on Wibro-Mimo," *Progress In Electromagnetics Research Letters*, Vol. 1, 77–83, 2008.

6. Chen, Y.-L., C. Ruan, and L. Peng, "A novel ultra-wideband bow-tie slot antenna in wireless communication systems," *Progress In Electromagnetics Research Letters*, Vol. 1, 101–108, 2008.
7. Kouveliotis, N. K. and C. Capsalis, "Prediction of the SAR level induced in a dielectric sphere by a thin wire dipole antenna," *Progress In Electromagnetics Research*, PIER 80, 321–336, 2008.
8. Khalatbari, S., D. Sardari, A. A. Mirzaee, and H. A. Sadafi, "Calculating SAR in two models of the human head exposed to mobile phones radiations at 900 and 1800 MHz," *PIERS Online*, Vol. 2, No. 1, 104–109, 2006.
9. Keshvari, J. and S. Lang, "Comparison of radio frequency energy absorption in ear and eye region of children and adults at 900, 1800 and 2450 MHz," *Physics in Medicine and Biology*, Vol. 50, 4355–4369, 2005.
10. Uduwawala, D., "Modeling and investigation of planar parabolic dipoles for GPR applications: A comparison with bow-tie using FDTD," *Journal of Electromagnetic Waves and Applications*, Vol. 20, No. 2, 227–236, 2006
11. Ding, W., Y. Zhang, P. Y. Zhu, et al., "Study on electromagnetic problems involving combinations of arbitrarily oriented thin-wire antennas and inhomogeneous dielectric objects with a hybrid MoM-FDTD method," *Journal of Electromagnetic Waves and Applications*, Vol. 20, No. 11, 1519–1533, 2006.
12. Wang, M. Y., J. Xu, J. Wu, et al., "FDTD study on scatterng of metallic column covered by double-negative metamaterial," *Journal of Electromagnetic Waves and Applications*, Vol. 21, No. 14, 1905–1914, 2007.
13. Fayedeh, H., C. Ghobadi, and J. Nourinia, "An improvment for FDTD analysis of thin-slot problems," *Progress In Electromagnetics Research B*, Vol. 2, 15–25, 2008.
14. Ali, M. and S. Sanyal, "FDTD analysis of rectangular waveguide in receiving mode as EMI sensors," *Progress In Electromagnetics Research B*, Vol. 2, 291–303, 2008.
15. Wang, J.-Q., O. Fujiwara, S. Watanabe, and Y. Yamanaka, "Computation with a parallel FDTD system of human-body effect on electromagnetic absorption for portable telephones," *IEEE Trans. on MTT*, Vol. 52, No. 1, 53–58, 2004.
16. Chen, X., D. Liang, and K. Huang, "Microwave imaging 3-D buried objects using parallel genetic algorithm combined with FDTD technique," *Journal of Electromagnetic Waves and Applications*, Vol. 20, No. 13, 1761–1774, 2006.

17. Guiffaut, C. and K. Mahdjoubi, "A parallel FDTD algorithm using the MPI library," *IEEE Antennas and Propagation Magazine*, Vol. 43, No. 2, 94–103, 2001.
18. Lei, J. Z., C. H. Liang, and Y. Zhang, "Study on shielding effectiveness of metallic cavities with apertures by combining parallel FDTD method with windowing technique," *Progress In Electromagnetics Research*, PIER 74, 85–112, 2007.
19. Zhou, X.-M., S.-L. Lai, and X.-L. Ni, "Numerical simulation on system of helical antenna handset and human head model," *Chinese Journal of Radio Science*, Vol. 19, No. 3, 329–332, 2004.
20. Yee, K. S., J. S. Chen, and A. H. Chang, "Conformal finite-difference time-domain (FDTD) with overlapping grids," *IEEE Trans. on AP*, Vol. 40, No. 9, 1068–1075, 1992.
21. Liu, Y., Z. Liang, and Z. Q. Yang, "A novel FDTD approach featuring two-level parallelization on PC cluster," *Progress In Electromagnetics Research*, PIER 80, 393–408, 2008.
22. Xu, F. and W. Hong, "Domain decomposition FDTD algorithm for the analysis of a new type of E-plane sectorial horn with aperture field distribution optimization," *IEEE Trans. on AP*, Vol. 52, No. 2, 426–434, 2004.
23. Mei, K. K. and J. Fang, "Superabsorption: a method to improve absorbing boundary conditions," *IEEE Trans. on AP*, Vol. 40, No. 9, 1001–1010, 1992.
24. Gabriel, C., "Compilation of the dielectric properties of body tissues at RF and microwave frequencies," *Brooks Air Force*, AL/OE-TR-1996-0037, San Antonio, TX, 1996.
25. "Protocol for the computational comparison of the SAM phantom to anatomically correct models of the human head," *IEEE SCC34/SC2/WG2*, Nov. 14, 2004.
26. Liu, Y., Z. Q. Yang, and Z. Liang, "Parallel computation strategy for the FDTD algorithm applied to HPM problems," *Proceedings of the First Euro-Asian Pulsed Power Conference*, Vol. 2, 717–720, Chengdu, China, Sep. 18–22, 2006.
27. Zhou, X.-M. and S.-L. Lai, "Numerical simulation of the interaction between the three dimension rotated human head model and handset monopole antenna," *Journal of South China University of Technology (Natural Science Edition)*, Vol. 32, No. 5, 30–33, 2004.